Received: 18 November 2022 | Revised: 17 December 2022 | Accepted: 25 December 2022
DOI: 10.22034/ecc.2022.370750.1557
Journal of Medicinal and Pharmaceutical Chemistry Research

FULL PAPER

Viologen molecular switches incorporating bis(acetylacetonato) cobalt(II) and bis(3-chloroacetylacetonato) cobalt (II) complexes

Hayder Hussain Ali[a,b,*] |**Wathiq Sattar Abdul-Hassan**[a]

[a]*Department of chemistry, College of science, University of Thi-Qar, 64001 Nassiria, Iraq*

[b]*Thi-Qar General Directorate of Education 64001 Nassiria, Iraq*

Cobalt(II) complexes: CoA and CoACl are synthesized. Treatment of CoA with 10 equivalents of 4,4-bipyridine (Bpy) in acetone afforded adduct complex CoA-Bpy. These three cobalt(II) complexes are characterized by FT-IR, mass and UV-Visible absorption spectrometries besides thermal and XRD analysis. The interactions of the complexes CoA and CoACl with Bpy to afford the adduct complexes are studied by UV-Visible absorption spectrometry. The interactions of the complexes CoA and CoACl with propylene linked bis-viologen ($V^{2+}A_2.2PF_6^-$) yield the adduct complexes coordination of $V^{2+}{}_2.2PF_6^-$ to cobalt(II) ion within cobalt(II) complexes. Then, switching motion of $V^{2+}{}_2.2PF_6^-$ coordinated to Co(II) ion was triggered by two electrons reduction.

***Corresponding Author:**
Hayder Hussain Ali
Email: hayderhusseinali4@gmail.com
Tel.: +9647811146081

KEYWORDS

Acetylacetone; cobalt complexes; adduct viologen; π-dimer.

Introduction

β-diketone compounds, whose the simplest and the most widely known member is pentane-2,4-dione (informally referred to as acetylacetone), have a number of very interesting and specific properties due to their structure (the presence of two carbonyl groups separated with one carbon atom) [1]. Their crucial feature is keto-enol tautomerism, the presence of ketone and the enol forms in equilibrium. The equilibrium in the case of β-diketones is strongly shifted towards the enol form due to the formation of the distinct resonance structure as a six-membered ring (Figure 1). Keto-enol equilibrium is affected by a number of other factors with the most important being solvent polarity and the presence and properties of substituents (both terminal ones and those in the methylene group). The capacity to form stable complexes with most metals is a direct consequence of the occurrence of such compounds in the enol form [2].

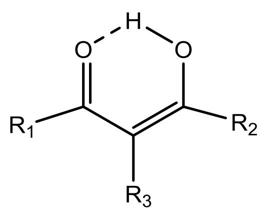

FIGURE 1 General structure of β-diketone [3]

β-diketones and their complexes have been used both in science and in industry. The compounds are frequently used in polymer technology e.g. as substrates for the manufacture of homogeneous and heterogeneous catalysts and as polymerisation catalysts (metal complexes) and substances which modifying the properties of resulting polymers (UV resistance and oxygen resistance). β-diketone complexes (especially with transition metals) are often used as catalysts of reactions, such as olefin oxidation, epoxidation, or olygomerisation [1,2]. They have also been widely used in healthcare, both as active pharmaceutical ingredients (or substrates for the manufacture of medicines) and cosmetic additives which reduce the detrimental effects of UV radiation on the skin. Furthermore, they are important for chemical analysis in which they are used for sample concentration (owing to their complexing activity), for air pollution monitoring (formaldehyde) or as stationary phases in gas chromatography (olein analysis). They are further employed as fuel additives, antiulcer and gastroprotective drugs [4], antiasthmatic and lung disease drugs [5,6], carcinogenic agents [4] and antidiabetic agents [7], fillers which improve polymer properties [8], substrates for the preparation of hydrophobic polymers [9], luminescent compounds [10], etc. Owing to their complexing properties, they are also used in environmental protection, e.g. for metal chelation in sewage [11]. The acac anion can act as a ligand towards metal ions, typically forming a bidentate complex where the metal is bound to the two oxygen atoms, thus forming a 6-membered ring. Metal acac compounds are typically isolated as crystalline solids that are neutral [12].

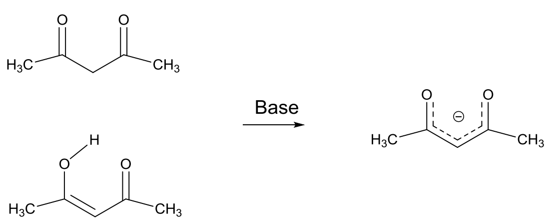

EQUATION 1 Keto-enol equilibrium of acetylacetone and formation of acetylacetonate anion [13]

In this work, we aimed to synthesize Cobalt (II) complexes with acetylacetone and 3-chloroacetylacetone and then their adduct complexes with 4,4'-bipyridine and propylene linked bis-viologen. After that, these adduct complexes can be employed in formation of molecular switches.

Experimental

Solvents and reagent

All the chemical materials and solvents are of chemically source, and used without further purification.

Apparatus

The FT-IR spectra are recorded using SHIMADZU/FT-IR Affinity-1 spectrophotometer and CsI disks in the department of Chemistry, College of Science, University of Thi-Qar. Mass spectra are recorded by using 5973 Network Mass Selective Detector manufactured by Agilent Technology (HP) with ion source of Electron Impact (EI) 70 ev in the Department of Chemistry, Tehran University, Iran. The thermal analysis and XRD were recorded on SDT Q600 V20, in Chemistry Department, Faculty of Science, University of Basra. The UV-visible absorption spectra are recorded on a T90+ UV-visible spectrometer (PG Instruments Ltd.) using conventional quartz cells having an optical path length of 1 cm, in the Department of Chemistry, College of Science, University of Thi-Qar.

Syntheses of bis(acetylacetone) cobalt(II), CoA, and bis(3- chloroacetylacetone) cobalt (II), CoACl

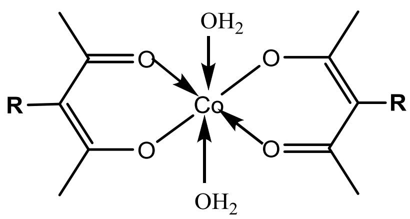

R = H: CoA, Cl: CoACl

Acetylacetone (3.2 mL, 31.3 mmol) or 3-chloroacetylacetone (3 mL, 25 mmol) is added slowly with stirring to a solution of

1.19 g, 29.7 mmol or 0.84 g, 21 mmol of sodium hydroxide in 10 mL of distilled water. The temperature during mixing should be kept below 40 °C. Any white solid formed at this step should be dissolved by extensive stirring or by addition of a few milliliters of distilled water. The resulted yellow solutions are added dropwise with vigorous stirring over a period of 2 hours to solutions of 3.8 g, 15.97 mmol or 3.2 g, 13.45 mmol of $CoCl_2.6H_2O$ dissolved in 20 mL or 10 mL respectively of distilled water. The resulting orange precipitates are collected by filtration and washed with 50 mL of distilled water. The moist solids are dissolved separately in a hot mixture of 39 mL ethanol (98 %) and 26 mL chloroform. The resulted red or gray solutions, respectively, are allowed to cool to lab temperature, and then cooled in ice bath. The orange needles are collected by filtration washed with 10 mL of cold ethanol (98%) and then air dried to afford respectively CoA in yield of 3.877 g, 83% (M.p.= 183 °C) or CoACl in yield of 3.1 g, 64% (M.p. =219 °C). FT-IR. cm^{-1} for CoA: 3549, 3394 υO-H of H_2O, 3100 υC-H of both aromatic and C=C-H, 2825 aliphatic υC-H, 1558 υC $\overset{---}{-}$ O +υC $\overset{---}{-}$ C, 1419 aliphatic C-H bending, 1310 υC-O acac, 659, 567 υCo-O. EI-MS (m/z) = 293$[M]^{+\bullet}$, 257$[M-2H_2O]^+$, 158$[M-acac-2H_2O]^+$. FT-IR, cm^{-1} for CoACl: 3417 υO-H of H_2O, 3074 υC-H of both aromatic and C=C-H, 2989, 2924 aliphatic υC-H, 1519 υC $\overset{---}{-}$ O + υC $\overset{---}{-}$ C, 1400 aliphatic C-H bending, 1261 υC-O acac, 659 υCo-O, 767 υC-Cl. EI-MS (m/z) = 362 $[M]^{+\bullet}$, 326$[M-2H_2O]^+$ and 192 $[M-2H_2O-Clacac]^+$.

Synthesis of CoA-Bpy

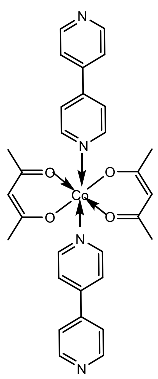

4,4'-bipyridine (1.63 g, 10 mmol) dissolved in 2 mL of acetone was added with stirring to CoA (0.5 g,1.7 mmol) dissolved in 3 mL of acetone. The mixture solution was stirred at lab temperature for 24 hours. The resulted precipitate was filtered and washed with acetone to afford CoA-Bpy as a yellow precipitate in yield of 0.622 g, 64% (M.p.= 206°C). FT–IR, cm^{-1}: 3055, 3001 υC-H of both aromatic and C=C-H, 2912 υC-H aliphatic, 1581 υC=N, 1516 υC $\overset{---}{-}$ O + υC $\overset{---}{-}$ C, 1404 aliphatic C-H bending, 1257 υC-O acac, 1080 υC-N, 671, 624 υCo-O, 509 υCo-N. EI-MS (m/z): 569$[M]^{+\bullet}$, 414 $[M-Bpy]^+$, 257$[M-2Bpy]^+$ and 156$[Co+acac]^+$.

Results and discussion

Mass spectrometry

The electron impact mass spectra of complexes: CoA, CoACl, and the adduct: CoA-Bpy was recorded and showed peaks occurred at m/z= 293, 362, and 569, respectively which were due to their molecular ions. These complexes structures were more confirmed by the appearance of other important peaks at m/z = 158, 192 and 257 which were attributed to loss of one acac and $2H_2O$, one acac-Cl and $2H_2O$, two bipyridine, respectively.

FT-IR Spectrometry

FT-IR Spectra of Cobalt(II) complexes: CoA, CoACl and the adduct complex CoA-Bpy are recorded and depicted in Figures 2, 3 and 4. The important bands with their assignments are listed in Experimental.

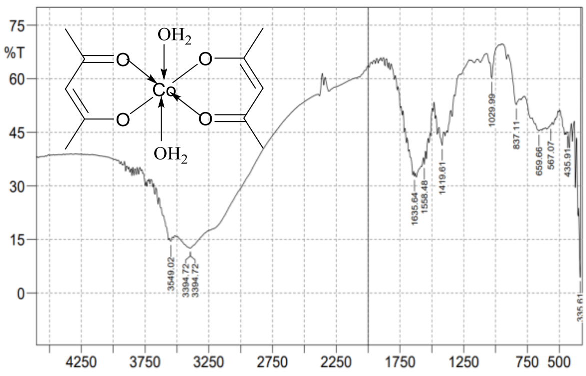

FIGURE 2 FT-IR spectrum of CoA

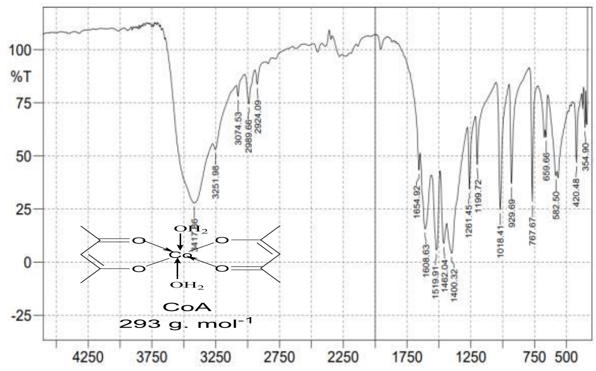

FIGURE 3 FT-IR spectrum of CoACl

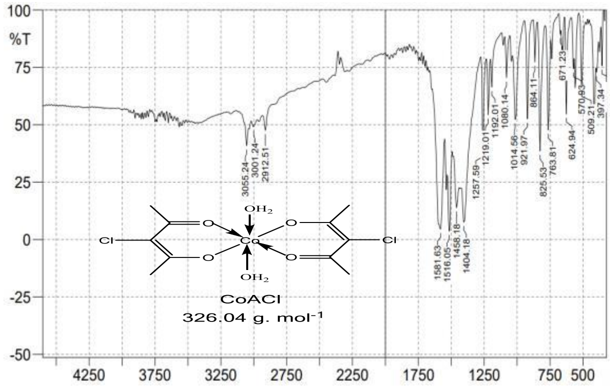

FIGURE 4 FT-IR spectrum of CoA-Bpy

The spectra were recorded using CsI pellets in the range of 300- 4500 cm^{-1}. FT-IR spectra of CoA, and CoACl show bands at 3394 cm^{-1} and 3251 cm^{-1} respectively which could be attributed to the stretching of H_2O molecules. This implies that a water molecule are present in the prepared complexes[3,14]. The aromatic C-H stretching and olifinic C-H stretching (C=C-H) occurred at 3100 cm^{-1}, 3074 cm^{-1} and both of 3055 cm^{-1} and 3001 cm^{-1} for CoA, CoACl and CoA-Bpy respectively. The metal complexes appeared bands at both of 2924 cm^{-1} and 2989 cm^{-1}, and 2912 cm^{-1} that can be attributed to $-CH_3$ asymmetric stretching of CoACl and CoA-Bpy respectively. The band at 1581 cm^{-1} of CoA-Bpy is assigned to C=N. The bands at 1558 cm^{-1}, 1519 cm^{-1}, and 1516 cm^{-1} of CoA, CoACl, and CoA-Bpy are assigned to υ C ⎓ C coupled with υ C ⎓ O and υ C ⎓ O coupled with υ C ⎓ C [15]. Methyl group appears showed bending vibrations at 1419 cm^{-1} of CoA and 1400 cm^{-1} of CoACl and 1404 cm^{-1} of CoA-Bpy[16]. The bands of complexes at 1261 cm^{-1} and 1257 cm^{-1} of CoACl and CoA-Bpy are attributed to coupled bending and stretching vibrations in the C-CO-C group. The bands at 1029 cm^{-1}, 1018 cm^{-1} and 1014 cm^{-1} are assigned to CH_3 rocking vibrations of CoA, CoACl and CoA-Bpy, respectively[12].

The FT-IR spectral data appeared at 837 cm^{-1}, 929 cm^{-1}, and 921 cm^{-1} are attributed to C ⎓ C coupled with C ⎓ O out-of-plane bend of CoA, CoACl and CoA-Bpy respectively. CoA shows bands at 659 cm^{-1}, 567 cm^{-1} and CoACl at 659 cm^{-1} and CoA-Bpy at 671 cm^{-1}, 624 cm^{-1} which can be assigned as υ Co-O[16]. The band at 767 cm^{-1} for CoACl is assigned to the stretching of C-Cl group. The stretching of Co-N group of the adduct CoA-Bpy is noted at 509 cm^{-1}.

Thermal analysis

The complexes CoA, CoACl, and CoA-Bpy were analyzed through TGA with a heating rate of 15 °C/min in nitrogen atmosphere to predict the nature of volatile compounds produced while heating in the temperature range of 0 to 600 °C [17]. The TG analysis curves of CoA, CoACl and CoA-Bpy are depicted in Figures 5, 6 and 7 respectively. The TG curves are presented in from of weight loss percentage versus temperature in Celsius. The decomposition patterns of the cobalt complexes CoA, CoACl and CoA-Bpy occur in three, three and one steps respectively. Both CoA and CoACl suffer three weight losses but with different weight loss behaviors (Table 2), during the two weight losses, CoA (70.63°C- 365.13°C) losses 74.005 from its structure while CoACl (75.11 °C- 356.10°C) losses 31.844 from its structure. During third weight loss of both complexes that ends at same temperature: ~ 599 °C, the weight losses are 80.852% and 40.885% from their structures respectively. Thus, CoACl is clearly more stable than CoA. The single weight losses of CoA-Bpy starts at 257.70°C which is higher than start temperature of first weight losses for CoA (at 70.63 °C) and CoACl (75.11 °C) respectively. This weight loss ends at 384.58°C which is lower than end temperature of second weight loss for both CoA (at 365.13 °C) and CoACl (at 356.10 °C), respectively. The CoA-Bpy losses 92.742 % from its structures lies decomposition of all the structure during its single weight loss compared with 74.005% and 31.849% for CoA and CoACl respectively. Therefore CoA-Bpy is loss much less stable than CoA and CoACl. The order of thermal stability of Cobalt complexes decreases in following sequence: CoACl > CoA > CoA-Bpy.

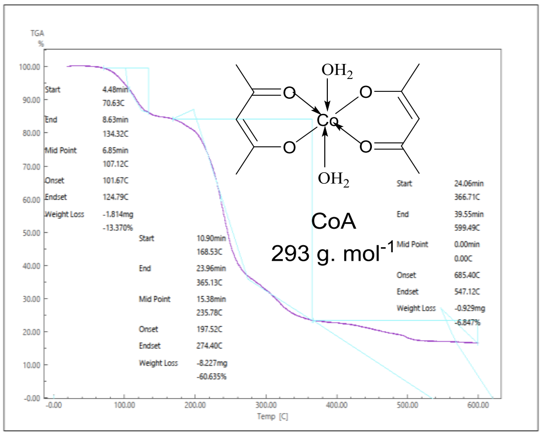

FIGURE 5 TGA of CoA

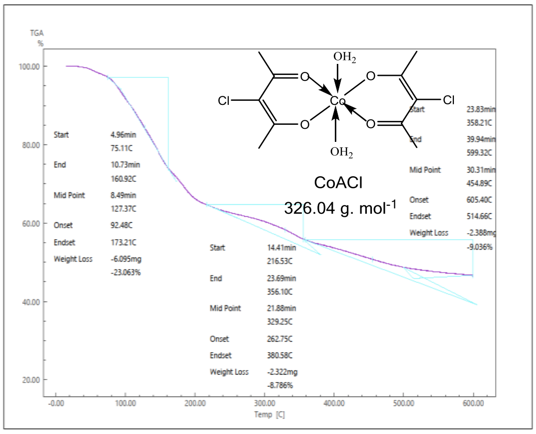

FIGURE 6 TGA of CoACl

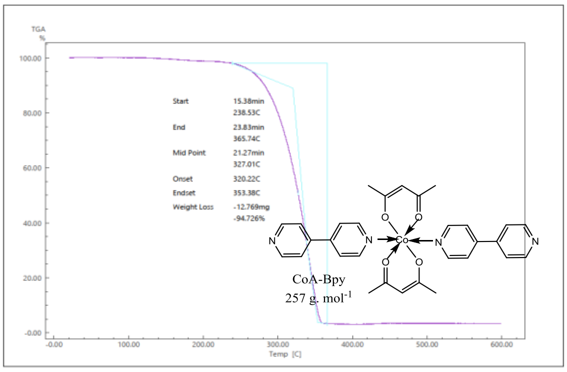

FIGURE 7 TGA of CoA-Bpy

TABLE 1 Thermogravimetric analysis data of the cobalt(II) complexes CoA, CoACl and CoA-Bpy

Compound M.wt (g.mol^{-1})	Temperature range (°C)	M.wt loss (g.mol^{-1}) Found	Calculated	Missing part	Residual part
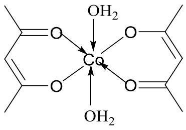 CoA 293 g. mol^{-1}	70.63-134.32	38.030	39.179	$2H_2O$ + 2H	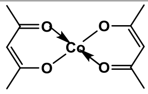
	168.53-365.13	76.040	77.040	$C_{10}H_{11}O_3$	CoOH
	366.71-599.49	58.933	56.111	OH	Co
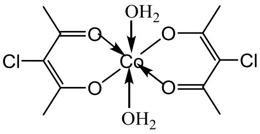 CoACl 326.04 g. mol^{-1}	75.11-160.92	83.830	83.250	2Cl + CH_3	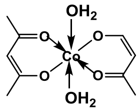
	216.53-356.1	32.619	31.714	H_2O +CH_3	$C_8H_{10}CoO_5$
	358.21-599.32	32.050	32.617	H_2O +CH_3	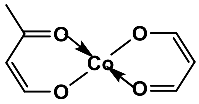
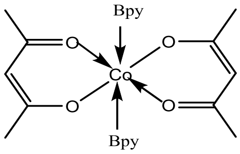 CoA-Bpy 569.53 g. mol^{-1}	238.53-365.74	566.49	530.48	$C_{29}H_{28}CoN_4O_3$	CH_2O

TABLE 2 Kinetic and thermodynamic parameters of each phase during the thermogravimetric analysis of Cobalt(II) complexes.

Complex	Phase No.	Temp. range (°c)	k (min^{-1})	$t_{1/2}$ (min)	Ea (J mol^{-1}) (*10^3)	A	ΔH (J mol^{-1}) (*10^3)	ΔS (J mol^{-1} K^{-1})	ΔG (J mol^{-1}) (*10^3)
CoA	1	70.63-134.32	0.04758	14.5649	60198.28	207.26	56814.36	-203.149	139496
	2	168.53-365.13	0.20089	3.4496	34522.97	22.59	29218.45	-225.32	172972.6
	3	366.71-599.49	0.24715	2.8039	19830.10	403.96	13328.32	-203.94	191160.8
CoACl	1	75.11-160.92	0.08711	7.9555	39663.3	79.99	37318.39	-211.58	110971.5
	2	216.53-356.10	0.06347	10.9185	7907.15	1.377	2677.46	-248.46	158958.8
	3	358.21-599.32	0.22307	3.1066	21610.11	4.477	14360.04	-241.37	224834.7
CoA-Bpy	1	238.53-365.74	0.4345	1.5949	119073.8	240.21	113769.28	-205.66	144980.4

It is clear from Table 2 that all weight loss phases are non-spontaneous endothermic reactions with losses in entopies [18].

X-ray diffraction

The XRD pattern of the complexes: CoA, CoACl, and CoA-Bpy are recorded and depicted in Figure 8.

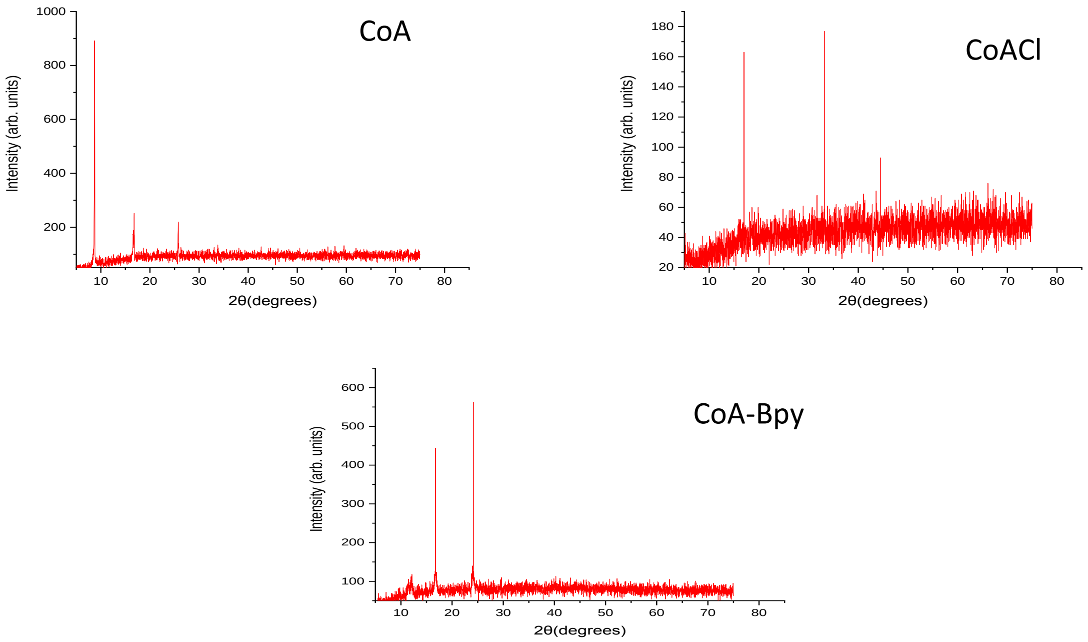

FIGURE 8 The XRD patterns of CoA, CoACl, and CoA-Bpy

The X-ray diffraction technique for powdered materials is an important method in the diagnosis of embedding complexes. Studies indicate that the reactants lose their characteristic peaks when the reaction occurs and the formation of new substances with different peaks. Therefore, this technique is one of the important techniques that indicate and confirm the formation of the complexes as well as inferring whether the resulting substance is crystalline or non-crystalline [19,20]. Plotted graph between βcosθ versus 4sinθ gives straight line with slope of strain (ε) and D equal to Kλ/ intercept, as depicted in Figure 9. The sizes of crystallite can be calculated using Sherrer-Debye Equation [21,22], which depends on the peaks of high intensity in calculating the sizes of crystals [23,24].

$$D = \frac{K\lambda}{\beta \cos\theta} \qquad (1)$$

Where, $D$the average crystal size, K: Scheerer's constant: 0.9, λ is the wavelength of the X-R ray source used: 1.5406 A°, β is the full width at the half maximum of the peak and θ is the diffracted angle of the peak.

The crystal size and lattice strain are also calculated by the Williamson Hall(W-H) method, Equation (2):

$$\beta \cos\theta = \frac{K\lambda}{D} + 4\varepsilon \sin\theta \qquad (2)$$

The XRD patterns are shown at angles 2θ = 5°-75°. The largest peaks are observed at 8.77 and 16.83, 33.198, 16.837, and 23.95 for CoA, CoACl and CoA-Bpy. The crystal size D and the strain ε are calculated from both Scherrer and Williamson-Hall methods and presented in Table 3.

From Table 3, the crystal size of CoA calculated from Williamson was 3.6 nm that was decreased to less than half value after substitution Cl atom instead of H atom in position 3 of ligand in CoACl compared with the complex CoA, while the addition of the axial ligand, Bpy to afford CoA-Bpy leads to increase of D value compared with its value in the precursor complex CoA.

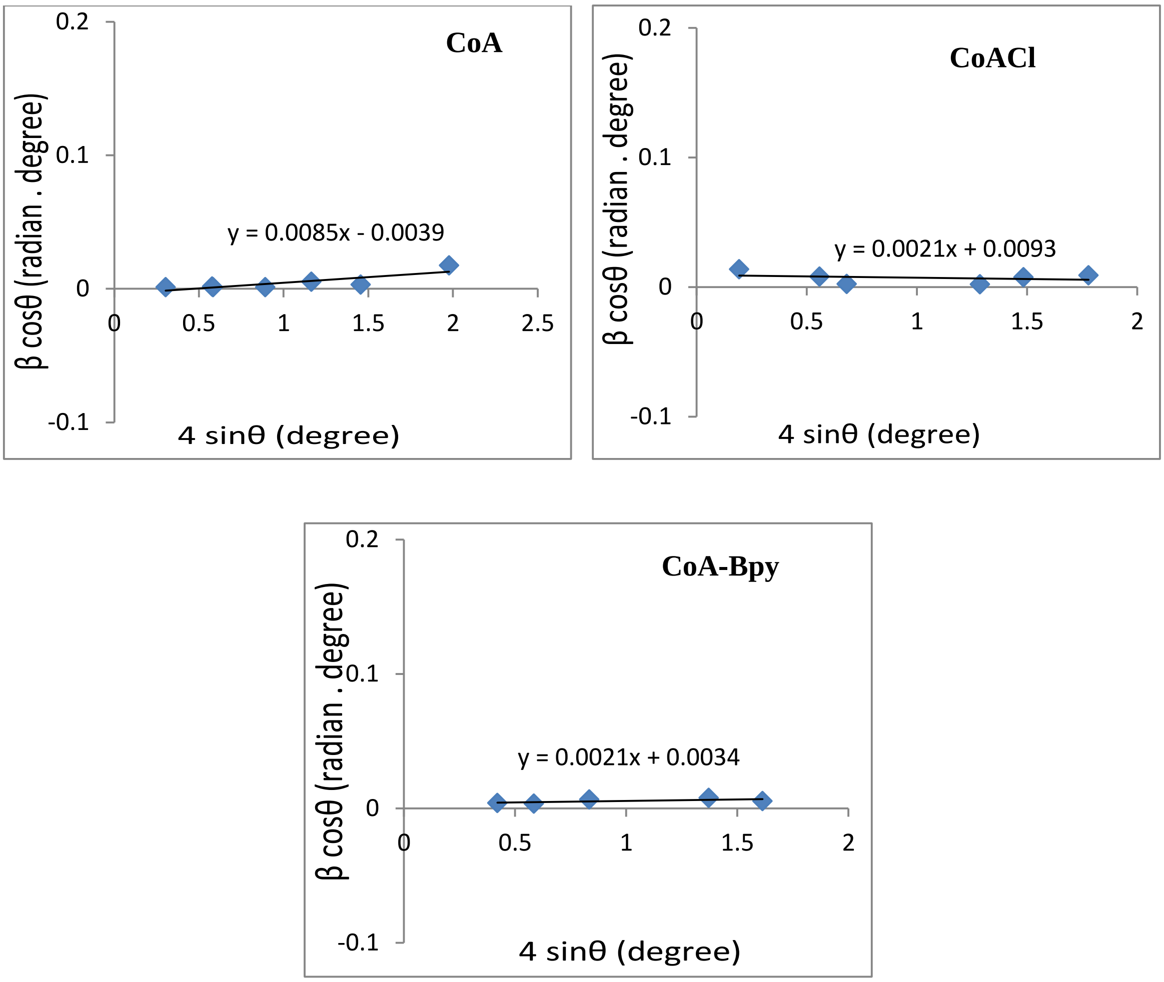

FIGURE 9 Williamson–Hall plot of the complexes: CoA, CoACl, and CoA-Bpy

TABLE 3 Values of crystallite sizes and strain according to Williamson-Hall model

complexes	Crystal size (D)		ε (Strain)
	Scherrer equation	Williamson-Hall equation	
CoA	11.6093	3.6	$8.5*10^{-3}$
CoACl	5.2363	1.5	$2.1*10^{-3}$
CoA-Bpy	4.8523	4.08	$2.1*10^{-3}$

UV-Visible absorption spectrometry in different solvents

The UV-Visible absorption spectra of cobalt(II) complexes: CoA, CoACl, and adduct: CoA-Bpy are recorded in three solvents (acetone, ethanol, and DMF) at two concentrations: low at 0.1 mM and high at 5 mM. The absorption spectra of low and high concentrations are performed to note clearly the UV and Visible absorption bands respectively of Cobalt(II) complexes [25]. The absorption spectra are depicted in Figure 10. The electronic absorption data are listed in Table 4 [26], [27,28].

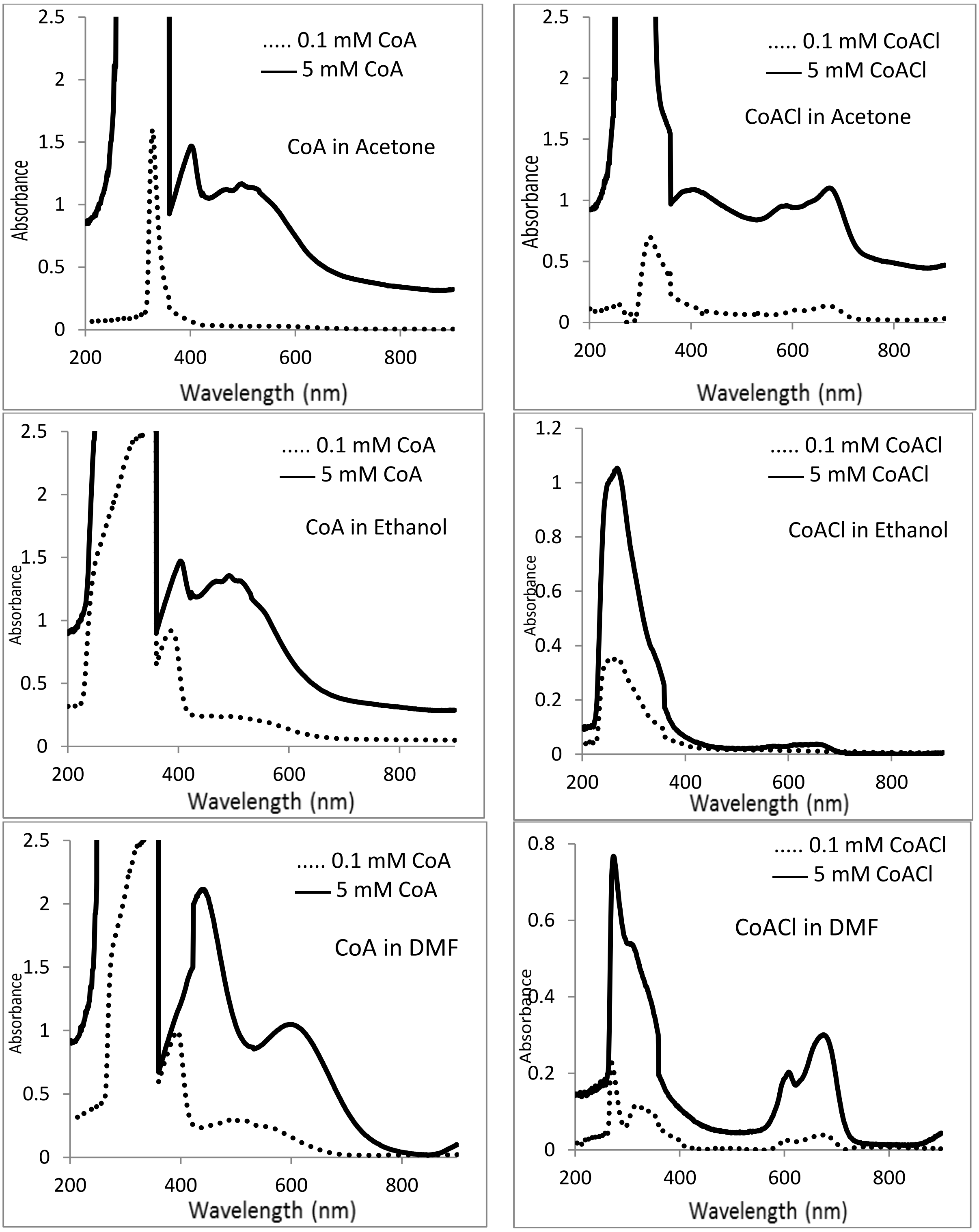
..... 0.1 mM CoA
—— 5 mM CoA
CoA in Acetone
Absorbance
Wavelength (nm)
..... 0.1 mM CoACl
—— 5 mM CoACl
CoACl in Acetone
Absorbance
Wavelength (nm)
..... 0.1 mM CoA
—— 5 mM CoA
CoA in Ethanol
Absorbance
Wavelength (nm)
..... 0.1 mM CoACl
—— 5 mM CoACl
CoACl in Ethanol
Absorbance
Wavelength (nm)
..... 0.1 mM CoA
—— 5 mM CoA
CoA in DMF
Absorbance
Wavelength (nm)
..... 0.1 mM CoACl
—— 5 mM CoACl
CoACl in DMF
Absorbance
Wavelength (nm)

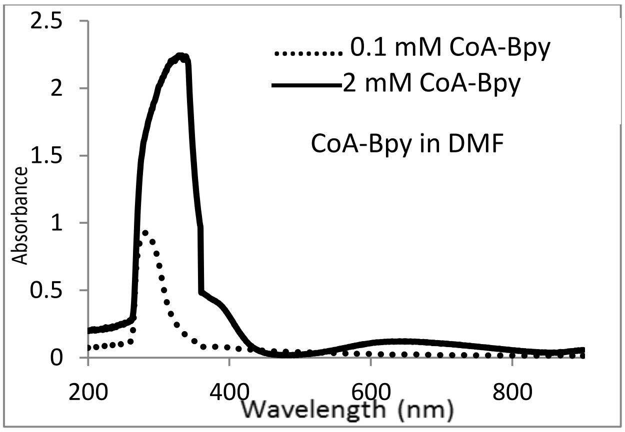

FIGURE 10 UV-Visible absorption spectra of CoA, CoACl, and CoA-Bpy complexes in DMF at r.t using quartz cell with path length of 1 cm

TABLE 4 The electronic absorption data of cobalt(II) complexes in different solvents

Complexes	λ_{max} in nm (ε, $M^{-1}.cm^{-1}$)	Solvent
0.1 mM CoA	328 (1605)	**Acetone**
5 mM CoA	401(293), 469(224.2), 502 (233), 535(217)	
0.1 mM CoACl	260(310), 294(102), 319 (702), 359 (399), 671 (136)	
5 mM CoACl	359 (309), 406 (218), 586(191), 673 (220)	
0.1 mM CoA	255 (15470), 333(24680), 386 (9170), 456(2430)	**Ethanol**
5 mM CoA	404 (294.4), 468(263), 492 (271.4), 519(258), 562(204)	
0.1 mM CoACl	268 (3540), 359(1010), 387(490)	
5 mM CoACl	253(201), 268 (211), 338(76), 572(6), 625(7), 655 (8)	
0.1 mM CoA	285(18100), 393 (9960), 496(3090), 570(2270)	**DMF**
5 mM CoA	442 (423), 597 (210)	
0.1 mM CoACl	270 (2270), 316(1160), 353(890) 359(780), 378(420), 474(60), 609 (260), 666 (390)	
5 mM CoACl	271(148), 608 (41), 313(106), 274 (153), 675 (60)	
0.1 mM CoA-Bpy	260 (9300), 359 (1080)	
2 mM CoA-Bpy	336 (1114), 390(190), 649 (61)	

The complex CoA showed a shoulder at 255 nm in ethanol and a peak at 328 nm in acetone which is red-shifted to 285 nm in DMF and 333 nm in ethanol, respectively. It showed also a peak occurred at 386 nm in ethanol that is red-shifted to 393 nm in DMF. It is noted a peak at 260 nm in acetone for CoACl that has been red-shifted to 268 nm and 270 nm in ethanol and DMF, respectively. Also, the peak at 319 nm of CoACl in acetone is blue-shifted and noted at 316 nm in DMF. Shoulders at 359 nm are noted in acetone, ethanol, and DMF (with the emergence of a shoulder at 353 nm). The shoulder at 387 nm in ethanol is noted at 378 nm (blue-shift) in DMF. The UV absorption bands of CoA are blue-shifted compared with those of CoACl that could be mostly correlated to a substitution of the electron-withdrawing chlorine atom in CoACl. The π-π* absorption transitions show bathochromic (red) shift in a more polar solvent, while there will be hypsochromic (blue) shift in n-π* transitions in a more polar solvent. Both these transitions get closer from each other's at increasing of solvent polarity. In addition, the π-π* transition of the higher intensity is expected to be merged with n-π* transition of the lowest intensity. The complexation with metals decrease a lot the chance of occurrence of n-π* transitions in complexes compared with their ligands. From the noted shifts in the UV absorption bands and their intensities of CoA and CoACl complexes, these transition bands could be attributed to the coincidence between n-π* and π-π* electronic transitions. In the visible region, three d-d transitions are normally expected for octahedral Cobalt(II) complexes which could be attributed to$^4T_{1g}$→$^4T_{2g}$ (F), $^4T_{1g}$→$^4A_{2g}$ (F), and $^4T_{1g}$(F)→ $^4T_{1g}$ (P). Four (401 nm, 469 nm, 502 nm, and 535 nm), five (404 nm, 468 nm, 492 nm, 519 nm, and 562 nm), and two (442 nm and 597 nm) d-d transition bands are noted for CoA in acetone, ethanol, and DMF, respectively. For CoACl, the d-d transitions are three (406 nm, 586 nm, and 673 nm), three (572 nm, 625 nm, and 655 nm), and two (608 nm and 675 nm) bands in acetone, ethanol, and DMF, respectively. The addition of ten equivalents of bipyridine to the CoA complex in DMF at lab temperature afforded immediately a yellow solid of CoA-Bpy. Unlike its precursor complex CoA, the resulted adduct CoA-Bpy is of different solubility; it is not soluble in organic solvents that dissolve CoA except DMF. Dramatic differences are noted in the UV-Visible spectrum of CoA-Bpy compared with those of CoA. The UV absorption spectrum of CoA-Bpy in DMF showed a peak at 260 nm (at 0.1 mM) that interestingly blue-shifted to 336 nm at increasing the solution concentration (at 2 mM). The second weak peak is noted around 390 nm. One broad d-d transition occurred at 649 nm that is red-shifted compared with that band at 597 nm of CoA. These differences noted in the electronic absorption spectrum of the adduct CoA-Bpy besides its different color and solubility compared with those of CoA support undoubtedly the formation of this adduct complex, i.e. the coordination of Bpy moiety to the cobalt(II) ion.

Interaction of cobalt(II) complexes with axial ligands (formation of adducts)

Interaction of CoA and CoACl as acceptors and 4'4-Bipyridine, Bpy as donor in DMF

The interaction of two concentrations (low and high) of complexes CoA and CoACl as acceptors with bipyrdine as donor in DMF are followed by UV-Visible absorption spectroscopy [29],[30] The absorption spectra are depicted in Figures 11 and 12, and Equation 2. The electronic absorption data are listed in Table 5.

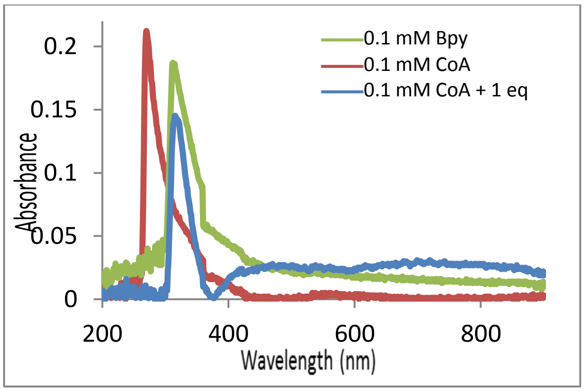

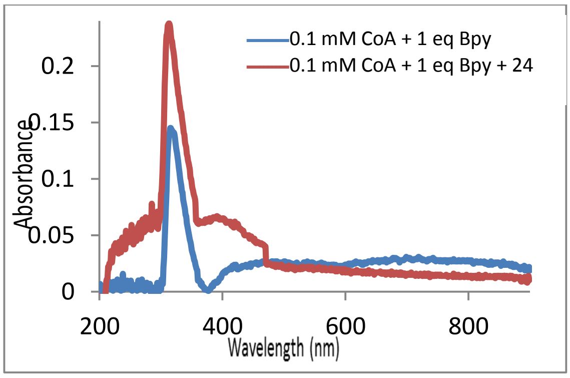

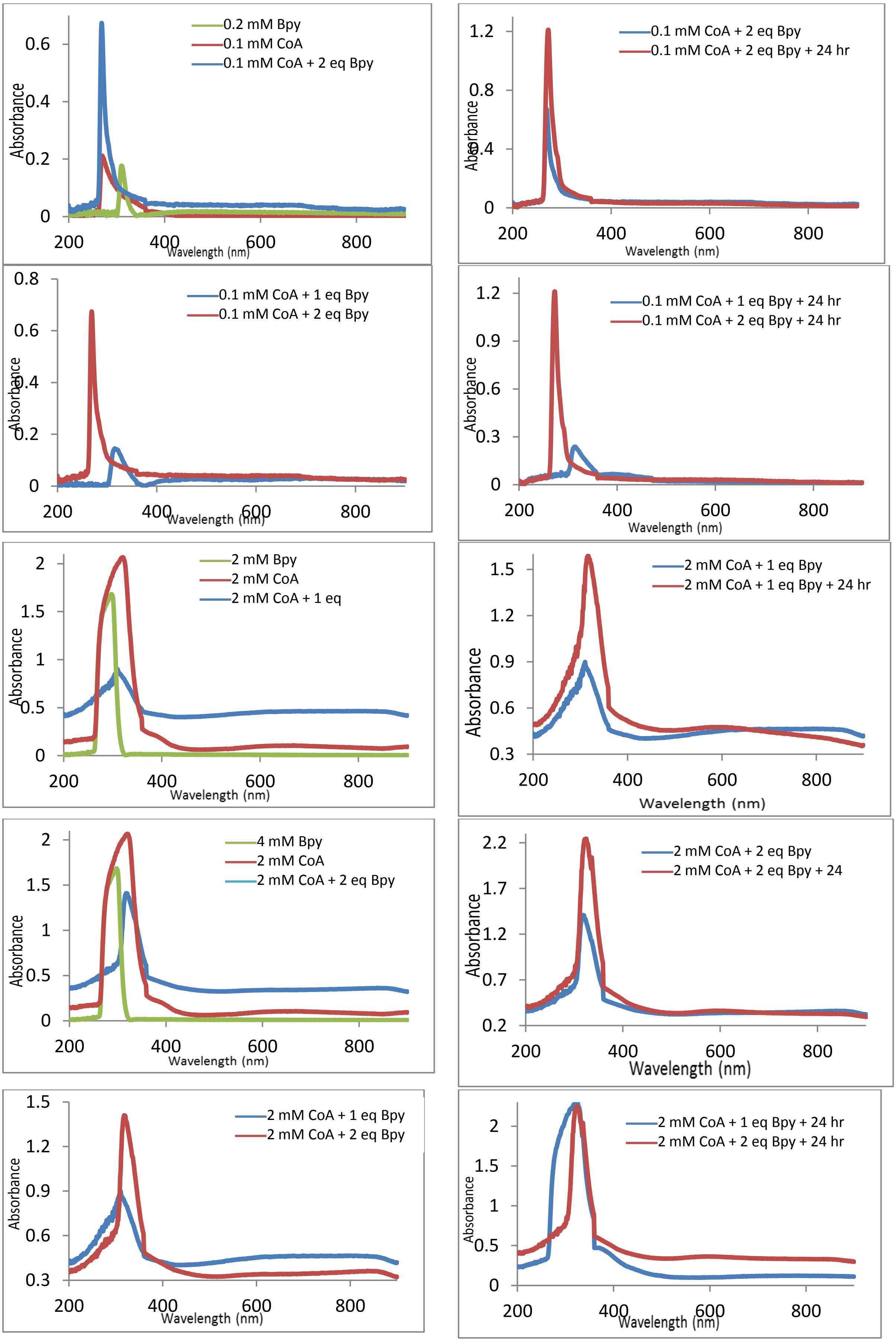

FIGURE 11 UV-Visible absorption spectra for different concentrations of CoA and Bpy and their mixture at mixing time after 24 hours from mixing in DMF at r.t. using quartz cell with a path length of 1 cm

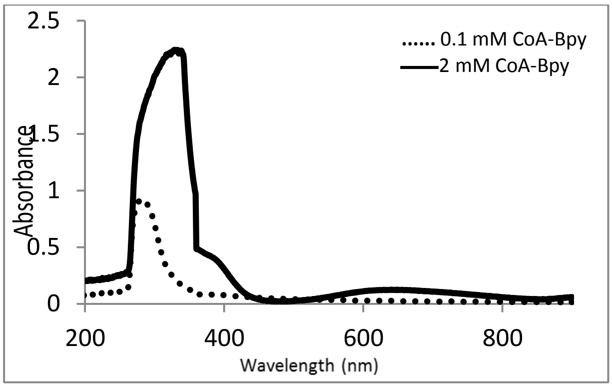

FIGURE 12 UV-Visible absorption spectra of 0.1mM CoA-Bpy (dotted line) and 2 mM CoA-Bpy (solid line) in DMF at r.t. using quartz cell with a path length of 1 cm

The UV-Visible spectrum of 0.1 mM CoA showed three absorption bands occurred at 269 nm, 418 nm, and 559 nm. After mixing with 1 eq of Bpy, red shifts are noted for the peaks at 269 nm and 418 nm of the complex to be at 315 nm and 422 nm in the mixture spectrum besides of appearance of new peak at 699 nm. The peaks of mixture occurred at 315 nm, 422 nm, and 699 nm are respectively shifted to 316 nm with increasing its intensity, shifted to 394 nm and disappeared after 24 hour from mixing with appearance of new peak at 526 nm. Also, important changes are noted between the absorption spectrum of 0.1 mM CoA with 2 eq Bpy and that after 24 hour from mixing. The UV-Visible spectrum of the concentrated 2 mM CoA showed absorptions at 321 nm, 359 nm, 390 nm, and 595 nm. After addition of 1eq Bpy, those absorptions happened at 287 nm (new), 310 nm (blue shifted), 359 nm, 387 nm (blue shifted), and 777 nm (new), respectively, and disappearance of the peak occurred at 595 nm of free CoA. At comparison of the absorption spectrum of the mixture with that after 24 hours, it is noted absorptions at 321 nm (red shifted), 369 nm (red shifted), and 592 nm (new), respectively. The mixture of 2 mM CoA with 2 eq of Bpy absorbed (compared with CoA) at 271 nm (new), 318 nm (blue shifted), 359 nm, disappearance of 595 nm and 837 nm (new). After 24 hours from mixing, these absorptions occurred at disappearance of 271 nm, 324 nm (red shifted), 336 nm (new), 359 nm, 390 nm (new), 588 nm (new), and disappearance of 837 nm. All noted absorption shifts in the UV-Visible spectra of mixtures of CoA (at low and high concentrations) with 1 or 2 equivalents of bpy support the formation of new absorbed species which is the adduct complex, i.e. coordination of Bpy moiety to Co(II) metal ion in CoA complex (Figure 13).

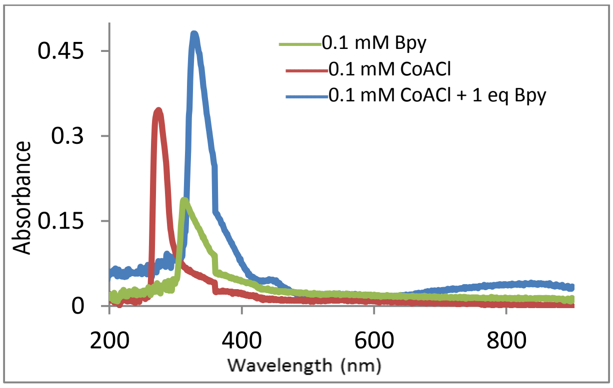

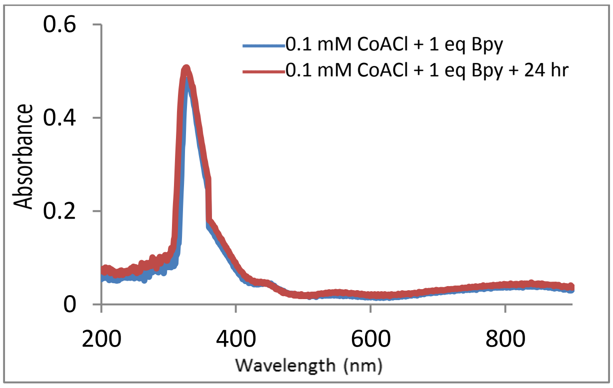

To be continued

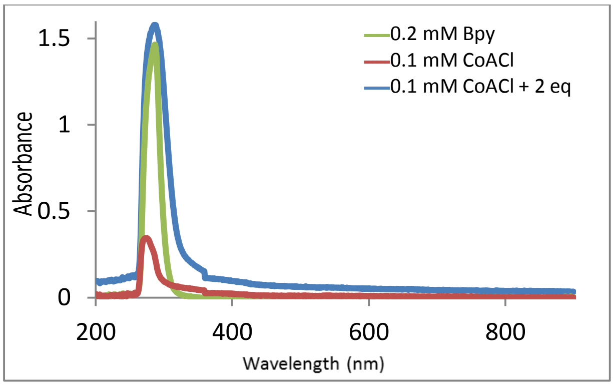
0.2 mM Bpy
0.1 mM CoACl
0.1 mM CoACl + 2 eq
Absorbance
Wavelength (nm)

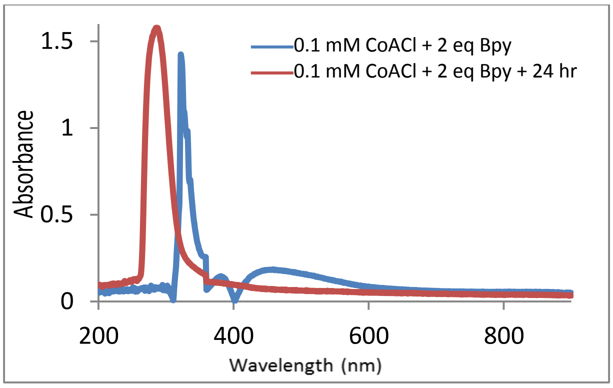
0.1 mM CoACl + 2 eq Bpy
0.1 mM CoACl + 2 eq Bpy + 24 hr
Absorbance
Wavelength (nm)

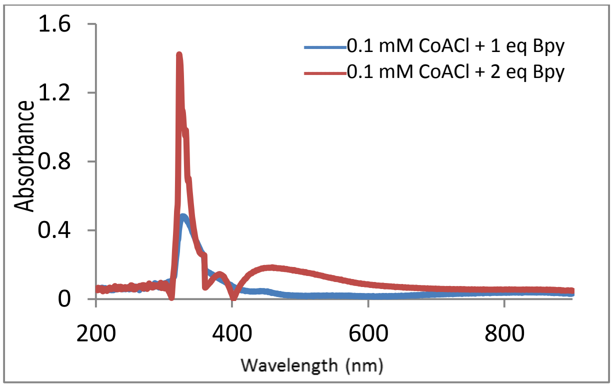
0.1 mM CoACl + 1 eq Bpy
0.1 mM CoACl + 2 eq Bpy
Absorbance
Wavelength (nm)

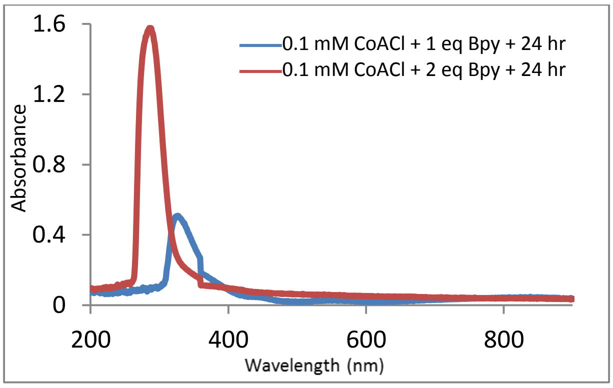
0.1 mM CoACl + 1 eq Bpy + 24 hr
0.1 mM CoACl + 2 eq Bpy + 24 hr
Absorbance
Wavelength (nm)

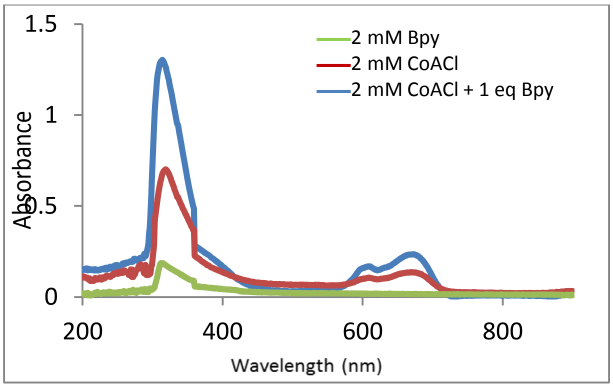
2 mM Bpy
2 mM CoACl
2 mM CoACl + 1 eq Bpy
Absorbance
Wavelength (nm)

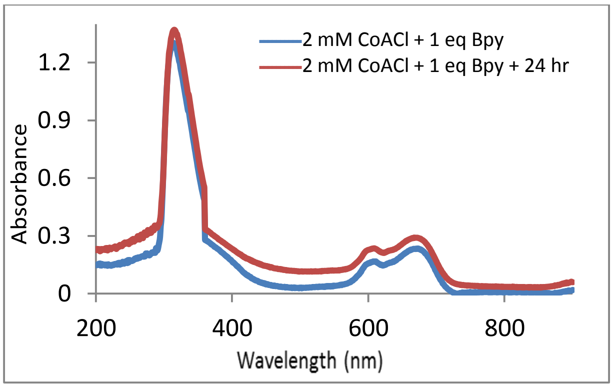
2 mM CoACl + 1 eq Bpy
2 mM CoACl + 1 eq Bpy + 24 hr
Absorbance
Wavelength (nm)

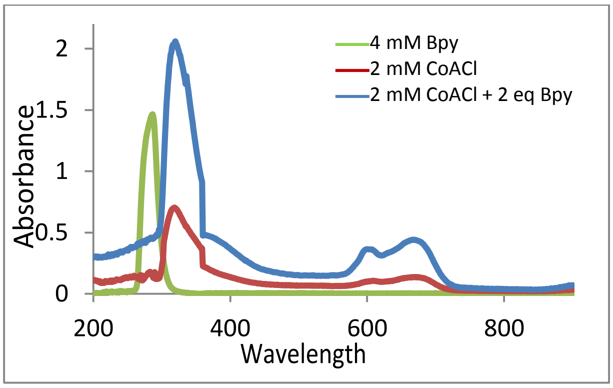
4 mM Bpy
2 mM CoACl
2 mM CoACl + 2 eq Bpy
Absorbance
Wavelength

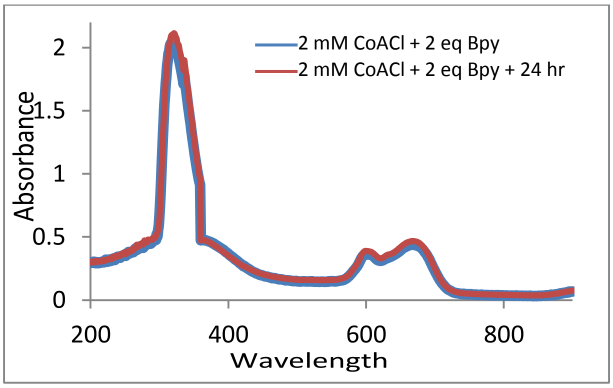
2 mM CoACl + 2 eq Bpy
2 mM CoACl + 2 eq Bpy + 24 hr
Absorbance
Wavelength

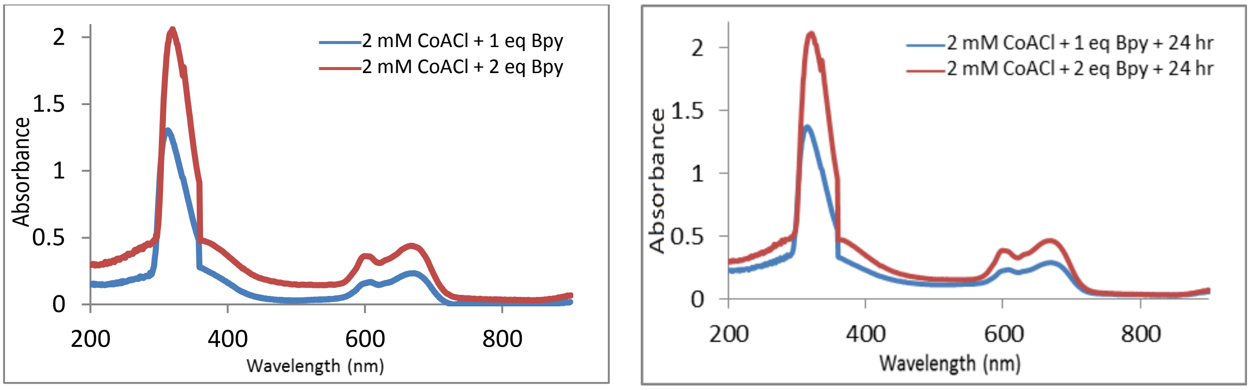

FIGURE 13 UV-Visible absorption spectra for different concentrations of CoACl and Bpy and their mixture at mixing time after 24 hours from mixing in DMF at r.t. using quartz cell with a path length of 1 cm

The 0.1 mM CoACl absorbed in DMF at 274 nm, 359 nm, 433 nm, and 541 nm after addition of 1eq Bpy, These absorptions Occurred at 330 nm (red shift), 359 nm, 367 nm (new), 454 nm (red shift), 563 nm (red shift) and 856 nm (new), respectively. After 24 hours from mixing (comparisons with last absorptions), the mixture showed absorptions at 327 nm (blue shift), 358 nm (blue shift), 437 nm (blue shift), 558 nm (blue shift), and 839 nm (red shift), respectively. Another important change is noted after addition 2eq of Bpy into CoA, the absorptions happened at 288 nm (red shift), 359 nm 382 nm (new), 454 nm (red shift), and 629 nm (new) compared with the spectrum of free CoA. To increase the interaction of Bpy with CoA, the spectrum is recorded after 24 hours from mixing and showed the absorptions 322 nm (blue shift), 339 nm (blue shift), 385 nm (red shift), 458 nm (red shift), and disappearance of 629 nm compared with the spectrum at mixing. At experiments with high concentration of CoACl, the uv-visible absorption spectrum of 2 mM CoACl showed the absorptions: 207 nm, 260 nm, 319 nm, 359 nm, 609 nm, and 671 nm. This absorption occurred at disappearance of 207 nm, 269 nm, 314 nm (blue shift), 359 nm, 387 nm (new), 609 nm, and 673 nm (red shift) after addition of 1eq of Bpy. After 24 hours of mixing, the spectrum included absorptions at 315 nm (red shift), 359 nm, disappearance of 387 nm, 604 nm, and 669 nm (blue shift) compared with the spectrum at mixing. Compared with the spectrum of 2 mM CoA, the spectrum of 2 mM CoA with 2eq of Bpy and that after 24 hours from mixing showed also big important changes in positions and intensities of absorptions. Compared the absorption spectra of mixtures of CoA or CoACl with Bpy, more dramatic changes in positions and intensities of the absorptions are noted for the mixtures of CoACl with Bpy. These higher changes could be related with big interaction among CoACl (Co(II) metal ion) with Bpy moieties.

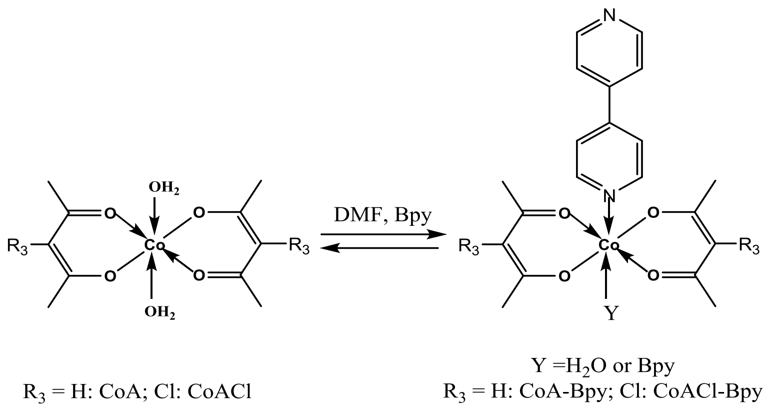

EQUATIONE 2 Formation of the adduct complexes: CoA-Bpy and CoACl-Bpy

TABLE 5 The electronic absorption data of 0.1 mM and 2 mM of both CoA and CoACl and their mixtures with 1 and 2 equivalents of Bpy in DMF

Compounds	λ $_{max}$ in nm (ε in $M^{-1}.cm^{-1}$)
0.1mM Bpy	312(1870) , 342(1220) , 409(420), 600(200), 639(190)
0.1 mM CoA	269(2120), 418(80), 559(50)
0.1 mM CoA + 1 eq Bpy	315, 359, 422, 699
0.1 mM CoA + 1 eq Bpy after 24 hr	316, 394, 526
0.2mM Bpy	619(80), 706(75), 728(70), 769(65), 889(105)
0.1 mM CoA + 2 eq Bpy	269, 425, 568
0.1 mM CoA + 2 eq Bpy after 24 hr	273 , 569 , 696
2mM Bpy	287(767), 481(29)
2 mM CoA	321(1033.5), 359(198), 390(102), 595(54)
2 mM CoA + 1 eq Bpy	287, 310, 359, 387, 777, 849
2 mM CoA + 1 eq Bpy after 24 hr	321, 336, 369, 592
4mM Bpy	298(420.75)
2 mM CoA + 2 eq Bpy	271, 318, 359, 837
2 mM CoA + 2 eq Bpy after 24 hr	324, 336, 359, 390, 588
0.1 mM CoACl	274(3460) , 359(420), 433(140), 541(120)
0.1 mM CoACl + 1 eq Bpy	330, 359, 367, 454, 563, 856
0.1 mM CoACl + 1 eq Bpy after 24 hr	327, 358, 437, 558, 839
0.1 mM CoACl + 2 eq Bpy	288, 359, 382, 454, 629
0.1 mM CoACl + 2 eq Bpy after 24 hr	322, 339, 385, 458
2 mM CoACl	207(52.5), 260(73), 319(351), 359(199.5), 609(53), 671(68)
2 mM CoACl + 1 eq Bpy	314, 359, 387, 673, 609
2 mM CoACl + 1 eq Bpy after 24 hr	315, 359, 609, 669
2 mM CoACl + 2 eq Bpy	320, 336, 359, 392, 602, 668
2 mM CoACl + 2 eq Bpy after 24 hr	321, 336, 359, 378, 602, 668

Interaction of CoA and CoACl as acceptors and bisviologen, $V_2^{2+}.2PF_6^-$ as donor in DMF

Low and high concentrations (0.1 mM and 2 mM) of each of CoA and CoACl are mixed with 1 or 2 equivalents of propylene-spacered bis-viologen, $V^{2+}A_2.2PF_6^-$ to assess the formation of adduct complexes, coordination of $V^{2+}A_2.2PF_6^-$ to Co(II) metal ion within CoA and CoACl structures. These interactions are followed by UV-Visible absorption spectrometry as presented in Figures 14 and 15 and Table 6.

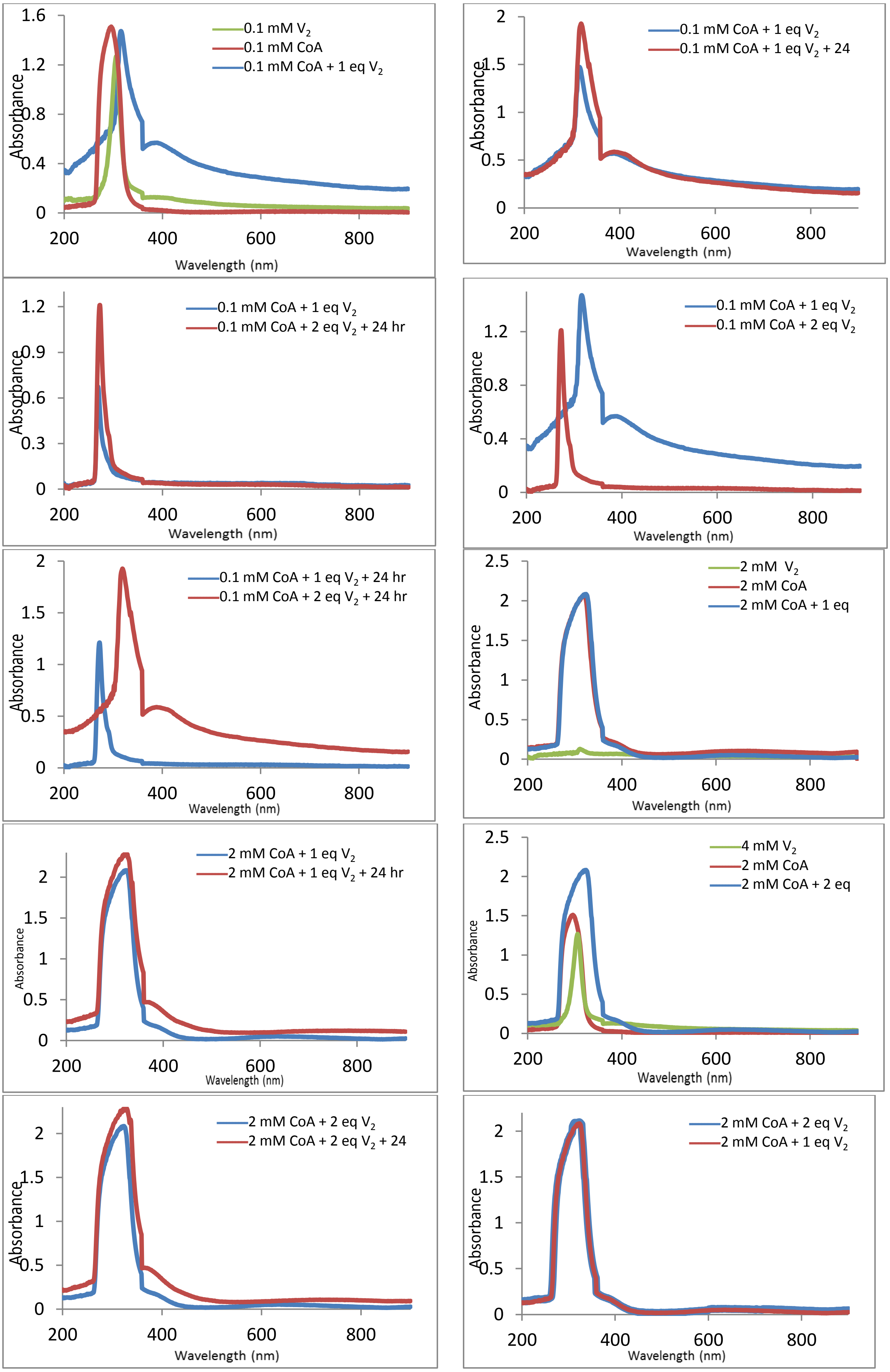
0.1 mM V2
0.1 mM CoA
0.1 mM CoA + 1 eq V2
0.1 mM CoA + 1 eq V2
0.1 mM CoA + 1 eq V2 + 24
0.1 mM CoA + 1 eq V2
0.1 mM CoA + 2 eq V2 + 24 hr
0.1 mM CoA + 1 eq V2
0.1 mM CoA + 2 eq V2
0.1 mM CoA + 1 eq V2 + 24 hr
0.1 mM CoA + 2 eq V2 + 24 hr
2 mM V2
2 mM CoA
2 mM CoA + 1 eq
2 mM CoA + 1 eq V2
2 mM CoA + 1 eq V2 + 24 hr
4 mM V2
2 mM CoA
2 mM CoA + 2 eq
2 mM CoA + 2 eq V2
2 mM CoA + 2 eq V2 + 24
2 mM CoA + 2 eq V2
2 mM CoA + 1 eq V2
Absorbance
Wavelength (nm)
200
400
600
800

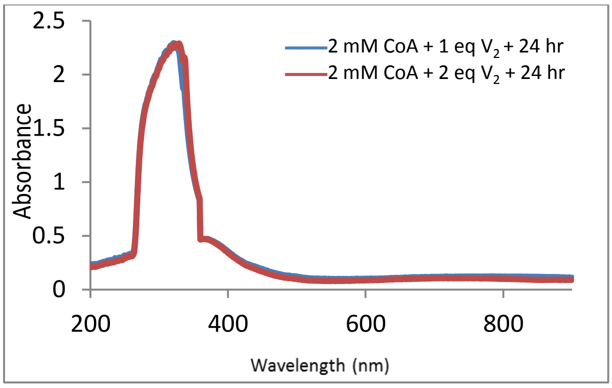

FIGURE 14 UV-Visible absorption spectra for different concentrations of CoA and V_2^{2+} and their mixture at mixing time after 24 hours from mixing in DMF at r.t. using quartz cell with a path length of 1 cm

The UV-Visible absorption spectrum of 0.1 mM CoA showed absorptions at 269 nm, 359 nm, 418 nm, and 559 nm that are noted at 316 nm (red shift), 359 nm, 390 nm (blue shift), and 637 nm (red shift), respectively, after mixing with 1 eq of $V_2^{2+}.2PF_6^-$. To increase the formation of the adduct $CoA.V_2^{2+}.2PF_6^-$, the mixture was kept for 24 hours from mixing, and then the spectrum is recorded. These spectrum contained absorptions at 319 nm (red shift), 336 nm (new), 359 nm, 389 nm (blue shift), and disappearance of peak at 637 nm compared with the spectrum at mixing. Compared with the mixture of 1 eq V_2^{2+}, the mixture of 2 eq showed absorptions at 269 nm (blue shift), 344 nm, 359 nm, 425 nm (red shift), 471 nm, and 610 nm (blue shift), respectively. After 24 hours from mixing the absorptions become 273 nm (red shift), 292 nm, 359 nm, disappearance of 471 nm, and 589 nm (blue shift), respectively. Comparisons spectra of 2 mM CoA, its mixture with 1eq Bpy and with that at 24 hours afforded absorptions 321 nm →324 nm (red shift) →321 nm (blue shift), no absorbance →no absorbance →336 nm (new), 359 nm →359 nm →359 nm, 389 nm →389 nm →386 nm, and 595 nm →636 nm, and (red shift) →797 nm (red shift), respectively. Likewise, important changes are noted in the spectrum after addition 2eq V_2^{2+} and the spectrum recorded after 24 hours compared with the spectrum of free CoA. These shifts and intensities noted for uv- and visible (d-d transition) absorptions after addition 1 or 2 equivalents of V_2^{2+}.2PF6- to CoA support undoubtedly the coordination of V_2^{2+} with Co(II) metal ion and formation of the adduct $CoA.V_2^{2+}.2PF_6^-$ [31].

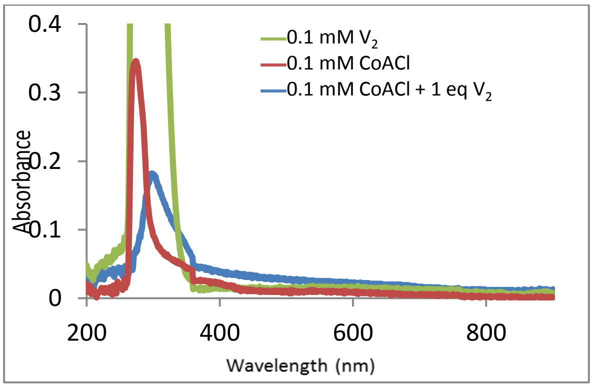

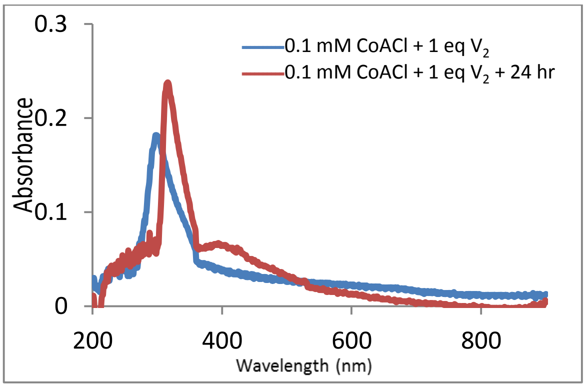

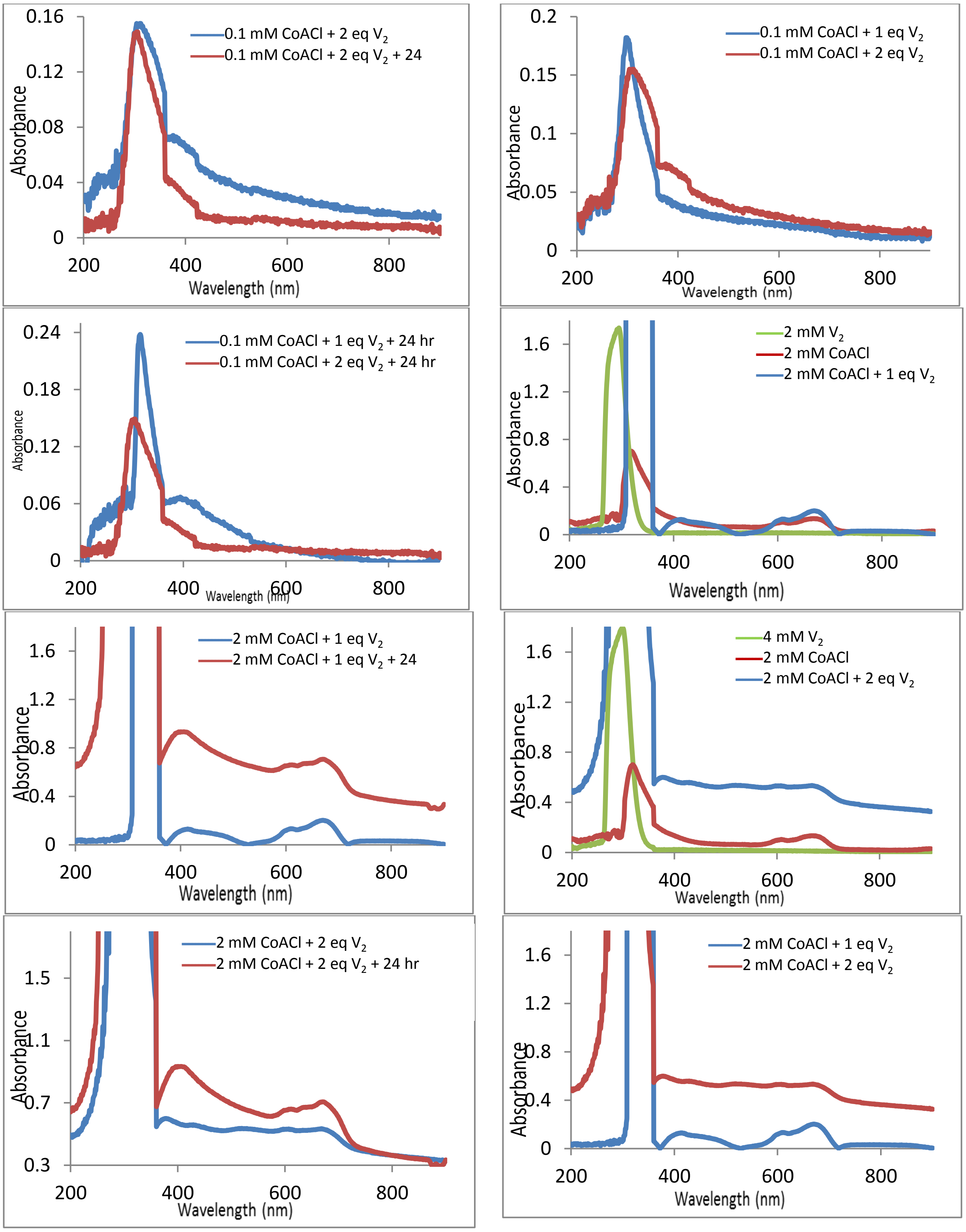
0.1 mM CoACl + 2 eq V_2
0.1 mM CoACl + 2 eq V_2 + 24
Absorbance
Wavelength (nm)
0.1 mM CoACl + 1 eq V_2
0.1 mM CoACl + 2 eq V_2
Absorbance
Wavelength (nm)
0.1 mM CoACl + 1 eq V_2 + 24 hr
0.1 mM CoACl + 2 eq V_2 + 24 hr
Absorbance
Wavelength (nm)
2 mM V_2
2 mM CoACl
2 mM CoACl + 1 eq V_2
Absorbance
Wavelength (nm)
2 mM CoACl + 1 eq V_2
2 mM CoACl + 1 eq V_2 + 24
Absorbance
Wavelength (nm)
4 mM V_2
2 mM CoACl
2 mM CoACl + 2 eq V_2
Absorbance
Wavelength (nm)
2 mM CoACl + 2 eq V_2
2 mM CoACl + 2 eq V_2 + 24 hr
Absorbance
Wavelength (nm)
2 mM CoACl + 1 eq V_2
2 mM CoACl + 2 eq V_2
Absorbance
Wavelength (nm)

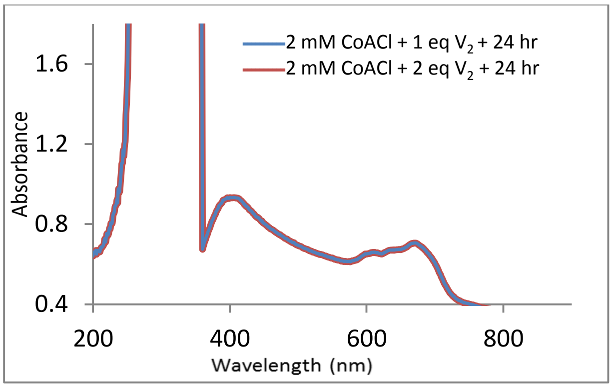

FIGURE 15 UV-Visible absorption spectra for different concentrations of CoACl and V_2^{2+} and their mixture at mixing time after 24 hours from mixing in DMF at r.t. using quartz cell with a path length of 1 cm

The absorptions of 0.1 mM CoACl occurred at 274 nm, 397 nm, 433 nm, and 541 nm are noted at 299 nm (new), 304 nm (red shift) disappeared, 446 nm (red shift) and 663 nm, respectively, after addition 1 eq of V_2^{2+} and formation of the adduct CoACl $V_2^{2+}.2PF_6^-$. After 24 hours from mixing, the last absorptions are seen at disappeared, 316 nm (red shift), 394 nm (new) disappeared, and 526 nm (blue shift) [12]. These changes could be related with the increase of adduct formation after 24 hours from mixing. The absorptions of 0.1 mM CoACl become after addition of 2 eq $V_2^{2+}.2PF_6^-$: 304 nm (red shift), 325 nm (new), 332 nm (blue shift) disappeared, and 537 nm (blue shift), respectively. After 24 hours from mixing, these absorptions occurred at 304 nm, 312 nm, 396 nm, 421 nm, and 575 nm. The concentrated solution of CoACl (2 mM) absorbed at 207 nm, 260 nm, 319 nm, 611 nm, and 671 nm. The visible spectrum of 2 mM CoACl with eq V_2^{2+} showed new peak at 416 nm besides two peaks at 613 nm and 671 nm which are red shifted and same position, respectively (with higher intensities) compared with the peaks at 611 nm and 671 nm of the free CoACl. The spectrum after 24 hours from mixing contained the absorptions at 400 nm (red shift), 611 nm (red shift), 635 nm (new), and 675 nm (red shift) with increase of intensities compared with those of the spectrum at mixing. These changes could be attributed to the increase of the adduct formation. Noticeable changes in both absorptions positions and intensities after addition of 2 eq of V_2^{2+} compared with the spectrum of the free CoACl. This is clearly consistent with the formation of the adduct complex with higher amount compared with the case of free CoACl and that after addition of 1 eq $V_2^{2+}.2PF_6^-$, respectively [29].

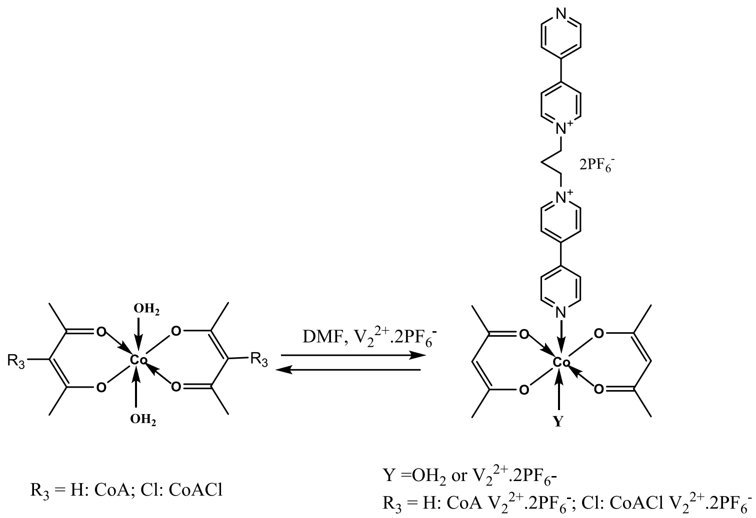

EQUATION 3 Formation of the adduct complexes CoA $V_2^{2+}.2PF_6^-$ and CoACl $V_2^{2+}.2PF_6^-$

TABLE 6 The electronic absorption data of 0.1 mM and 2 mM of both CoA and CoACl and their mixtures with 1 and 2 equivalents of $V_2^{2+}.2PF_6^-$ in DMF

Compounds	λ_{max} in nm (ε in $M^{-1}.cm^{-1}$)
0.1 mM V_2	306(12680), 359(1630), 382(1280), 566(780)
0.1 mM CoA	269(2120), 359(470), 418(80), 559(50)
0.1 mM CoA + 1 eq V_2	316, 359, 390, 637
0.1 mM CoA + 1 eq V_2 after 24 hr	319, 336, 359, 389
0.2mM V_2	311(885), 352(40), 518(95)
0.1 mM CoA + 2 eq V_2	269, 425, 610
0.1 mM CoA + 2 eq V_2 after 24 hr	273, 292, 359, 589
2 mM V_2	311(65), 389(34.5), 507(25), 668(18.5)
2 mM CoA	321(1033.5), 595(54)
2 mM CoA + 1 eq V_2	324, 391, 636
2 mM CoA + 1 eq V_2 after 24 hr	321, 336, 792
4 mM V_2	306(317) , 590(16.5)
2 mM CoA + 2 eq V_2	323, 359, 386, 396, 607, 637, 737
2 mM CoA + 2 eq V_2 after 24 hr	329 , 336, 359, 366 , 613, 697
0.1 mM CoACl	274(3460) , 359(410), 397(220), 433(140), 541(120)
0.1 mM CoACl + 1 eq V_2	299, 304, 359, 446, 663
0.1 mM CoACl + 1 eq V_2 after 24 hr	316, 359, 394, 526
0.1 mM CoACl + 2 eq V_2	304, 325, 332, 359, 376, 537
0.1 mM CoACl + 2 eq V_2 after 24 hr	304, 312, 358, 396, 421, 575
2 mM CoACl	207(52.5), 260(73), 319(351), 359(199.5), 611(52), 671(68)
2 mM CoACl + 1 eq V_2	415, 613, 671
2 mM CoACl + 1 eq V_2 after 24 hr	400, 611, 635, 675
2 mM CoACl + 2 eq V_2	377, 359, 377, 433, 520, 604, 669
2 mM CoACl + 2 eq V_2 after 24 hr	406, 609, 635, 670

Reduction of mixtures of each of CoA and CoACl with $V_2^{2+}.2PF_6^-$ (formation of molecular switches)

The mixture solutions of the adducts CoA.$V_2^{2+}.2PF_6^-$ and CoACl.$V_2^{2+}.2PF_6^-$ are reduced by activated zinc powder under argon atmosphere as presented in Figures 16 to 19.

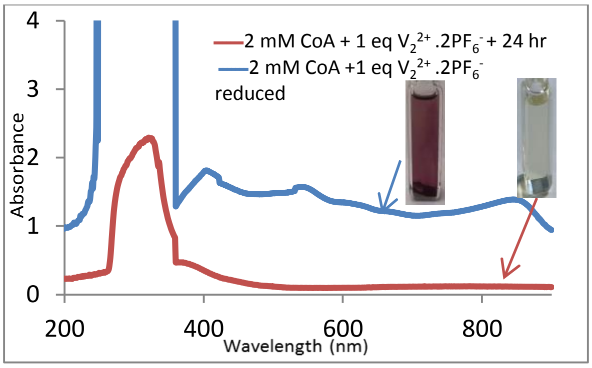

FIGURE 16 UV-Visible absorption spectra of mixtures of 2 mM CoA with 1eq V_2 after 24 hours from mixing (red line) and the same mixture reduced (blue line) in DMF at r.t. using quartz cell with a path length of 1 cm

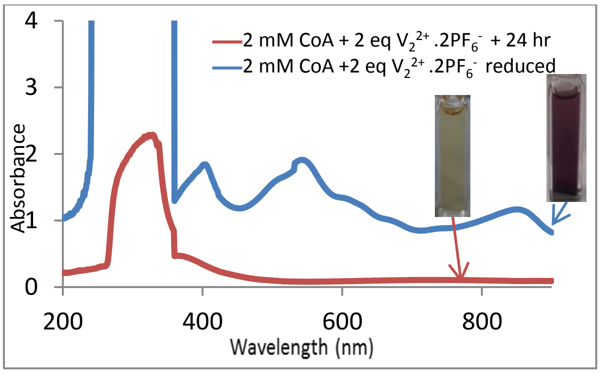

FIGURE 17 UV-Visible absorption spectra of mixtures of 2 mM CoA with 2eq V^{2+} after 24 hours from mixing (red line) and same mixture reduced (blue line) in DMF at r.t. using quartz cell with a path length of 1 cm

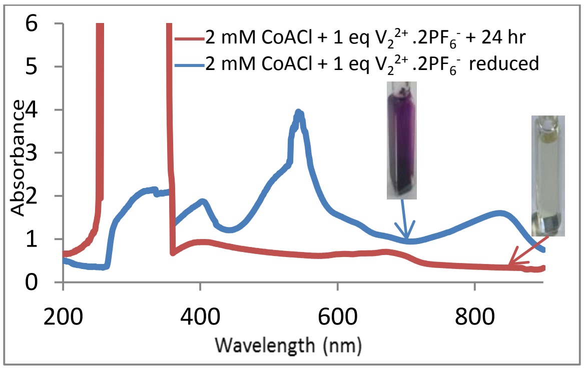

FIGURE 18 UV-Visible absorption spectra of mixtures of 2 mM CoACl with 1eq V_2 after 24 hours from mixing (red line) and the same mixture reduced (blue line) in DMF at r.t. using quartz cell with a path length of 1 cm

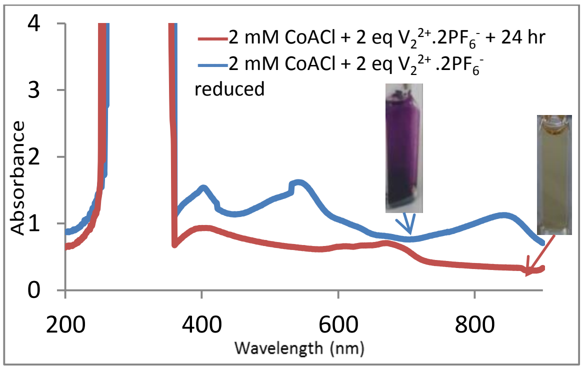

FIGURE 19 UV-Visible absorption spectra of mixtures of 2 mM CoACl with 2eq V_2 after 24 hours from mixing (red line) and the same mixture reduced (blue line) in DMF at r.t. using quartz cell with a path length of 1 cm

The reduced mixture of CoA + 1 eq $V_2^{2+}.2PF_6^-$ showed the absorptions 405 nm, 498 nm, 543 nm, 612 nm, and 845 nm. Likewise, the reduced mixture of CoA + 2 eq $V_2^{2+}.2PF_6^-$ absorbed at 404 nm, 503 nm, 542 nm, 608 nm, 672 nm, 740 nm, and 848 nm. The absorptions at 405 nm, 612 nm, 404 nm, 608 nm, 672 nm, and 740 nm for both reduced mixtures are attributed to non-dimerized viologen radicals of $V_2^{2+}.2PF_6^-$ in the adduct complex. While the absorptions occurred at 543 nm, 845 nm, 542 nm, and 848 nm are assigned to dimerized V_2^{2+} in the adduct complex CoA $V_2^{2+}.2PF_6^-$. The reduced mixture of CoACl + 1 eq $V_2^{2+}.2PF_6^-$ showed the absorptions of 401 nm, 617 nm, and 674 nm. The reduced mixture of CoACl + 2 eq $V_2^{2+}.2PF_6^-$ showed the absorptions 403 nm, 622 nm, and 681 nm. All those mentioned absorptions for both reduced mixtures are undoubtedly assigned to non-dimerized viologen radicals of $V_2^{2+}.2PF_6^-$ in the adduct complex. Moreover, the reduced mixtures of CoACl+1eq $V_2^{2+}.2PF_6^-$ and CoACl +2 eq $V_2^{2+}.2PF_6^-$ showed the absorptions 542 nm, 837 nm, 542 nm, and 846 nm, respectively. Those absorptions are related with the dimerized viologen radicals within the structure of the adduct CoACl.$V_2^{2+}.2PF_6$- [31,12] (Equation 4).

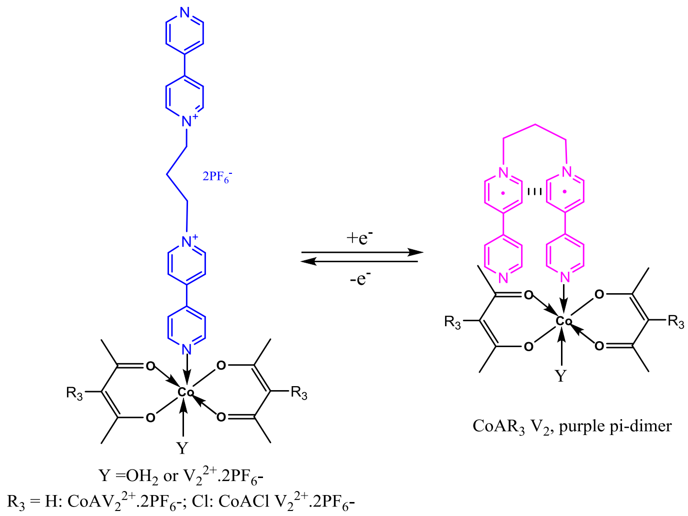

EQUATION 4 Molecular switches based on the adducts of $V_2^{2+}.2PF_6^-$ and CoAR$_3$ $V_2^{2+}.2PF_6^-$ complexes in DMF

TABLE 7 The electronic absorption data for 2 mM of both CoA and CoACl and their non-reduced and reduced mixtures with 1 and 2 equivalents of $V_2^{2+}.2PF_6^-$ in DMF

Mixture	λ_{max}
2 mM CoA + 1 eq V_2 after 24 hr	792, 336, 321
reduced 2 mM CoA + 1 eq V_2	845, 610, 540, 405
2 mM CoA + 2 eq V_2 after 24 hr	329 , 336, 359, 366 , 613, 697
reduced 2 mM CoA + 2 eq V_2	848, 740, 672, 608, 542, 503, 404
2 mM CoACl + 1 eq V_2 after 24 hr	675 , 635, 611, 400
reduced 2 mM CoACl + 1 eq V_2	837, 674, 617, 542, 401, 359, 330
2 mM CoACl + 2 eq V_2 after 24 hr	670, 635, 609, 406
reduced 2 mM CoACl + 2 eq V_2	846, 681, 622, 542, 403

Conclusion

The reaction of acetylacetone or 3-Chloro acetylacetone with Co(II) ion results in the cobalt complexes. The reaction of the complex CoA with ten equivalents of 4,4'-bipyridine (Bpy) in ne afford the adduct complex CoA-Bpy. The structures of these cobalt(II) complexes are characterized by different techniques. The FT-IR spectroscopy confirmed the coordination of H_2O molecules in CoA, CoACl, and Bpy in CoA-Bpy. The stretching of Co-O and Co-N groups is noted in FT-IR spectra. Mass spectra showed the molecular ions of these complexes besides other important peaks that well-confirmed the structures. Thermal analyses showed that the order of thermal stability of cobalt complexes decrease in following sequence CoACl> CoA> CoA-Bpy. All TG phases are first order reactions. The kinetic and thermodynamic parameters are calculated for each phase during the thermal analyses. Values obtained for each phase proved that all phases are non-spontaneous endothermic reactions. Based on the XRD data, crystal sizes D are calculated from both Scherer and Williamson-Hall methods. Furthermore, the strain values are calculated from the last method. It was found that D for CoA is larger than that of CoACl, while the substitution of Bpy in CoA-Bpy instead of H_2O in CoA increased D value. The UV-Visible absorption spectra of cobalt(II) complexes in different solvents showed transitions attributed to π-π* merged with n-π* absorptions. The d-d transitions have been perfectly shown. The formation of the adduct CoA-Bpy is confirmed by comparison of its spectra with those of the precursor CoA. The formation of the adduct complexes from interactions of CoA and CoACl with Bpy are followed by UV-Visible absorption spectroscopy. The $V^{2+}A_2.2PF_6^-$ units in these adducts are reduced by two electrons to afford dimerized V_2 within adduct complexes structures.

Acknowledgements

The authors would like to present the sincere appreciation to the supervisors, the assistant professor, Dr. Wathiq Sattar, who presented valuable information and supported throughout the research period. Also, the authors would like to thank Prof. Dr. Ibrahim Abboud for his support during the research period.

Conflict of Interest

We have no conflicts of interest to disclose.

Orcid:

Hayder Hussain Ali:

https://orcid.org/0009-0006-9805-8447

Wathiq Star Abdul-Hassan:

https://orcid.org/0000-0003-1297-3822

References

[١]A. Mannan, S. Abbas, T. Noor, M. Nawaz, New 3-D Mn(II) coordination polymer with redox active oxalate linker; an efficient and robust electrocatalyst for oxygen evolution reaction, *Inorganica Chim. Acta*., **2021**, *514*, 119982. [Crossref], [Google Scholar], [Publisher]

[٢]W. Urbaniak, K. Jurek, K. Witt, A. Goraczko, B. Staniszewski, Properties and application of diketones and their Derivatives, *Chemik*., **2011**, *65*, 273–282. [Google Scholar], [Publisher]

[٣]S.G. Yiase, S.O. Adejo, S.T. Iningev, Manganese (II) and Cobalt (II) Acetylacetonates as Antimicrobial Agents, *Niger. Ann. Pure Appl. Sci*., **2019**, *1*, 176–185. [Crossref], [Google Scholar], [Publisher]

[4] R.K. Sodhi, S. Paul, An overview of metal acetylacetonates: developing areas/routes to new materials and applications in organic syntheses, *Catal. Surv. from Asia*., **2018**, *22*, 31–62. [Crossref], [Google Scholar], [Publisher]

[٥]F. Dolati, S.F. Tayyari, M. Vakili, A. Ebrahimi, Vibrational spectra of α-bromo and α-chloro derivatives of tris(acetylacetonato)chromium(III), *J. Mol. Struct*., **2016**, *1103*, 1–8. [Crossref], [Google Scholar], [Publisher]

[6] I.A. Jassem, W.S. Abdul-Hassan, I.A. Flafel, S.A. Ali, Z.M. Mahdi, Cloud Point and Solvent Extraction of Copper (II) by Bis(3-chloroacetylacetone) Ethylenediamine, *J. Med. Chem. Sci*., **2022**. [Crossref], [Google Scholar], [Publisher]

[7] D.S. Kadam, Sudhakar G Patil, D. Mammen, S.D. Kadam, V.S. More, In Silico molecular docking against-KIT tyrosine kinase and ADME studies of 4-thiazolidinone derivatives, *Chemik*, **2011**, *65*, 273–282. [Crossref], [Pdf], [Publisher]

[18] W. Qin, D. Peng, X. Wu, J. Liao, Study on the resistance performance of TiO2/cyanate ester nano-composites exposed to electron radiation, *Nucl. Instruments Methods Phys. Res. Sect. B Beam Interact. with Mater. Atoms*., **2014**, *325*, 115–119. [Crossref], [Google Scholar], [Publisher]

[9] U. Schubert, Silica-based and transition metal-based inorganic-organic hybrid materials—a comparison, *J. Sol-Gel Sci. Technol*., **2003**, *26*, 47–55. [Crossref], [Google Scholar], [Publisher]

[10] S.B. Meshkova, The dependence of the luminescence intensity of lanthanide complexes with β-diketones on the ligand form, *J. Fluoresc*., **2000**, *10*, 333–337. [Crossref], [Google Scholar], [Publisher]

[11] A.S. El-Tabl, M.M. Gharieb, H.S. Hemida, S.M. Faheem, Synthesis, structural characterization and antimicrobial study on metal complexes of new bioactive ligand with terminal wings, *J. Chem. Chem. Sci*., **2020**, *10*, 65–85. [Google Scholar], [Publisher]

[12] A.H. Gatea, W.S. Abdul-Hassan, S.A. Ali, Z.M. Mahdi, Ligand adducts of bis(acetylacetonato) copper(II), bis(3-chloroacetylacetonato) copper(II) with 4,4'-bipyridine, and propylene spacered bis-viologen, *J. Med. Chem. Sci*., **2023**. [Crossref], [Google Scholar], [Publisher]

[13] M. Saeed, R. Saleem, Synthesis and chemical characterization of metals (Al, Cr, Co, Mn and VO) complexes with acetylacetone (β-diketone), **2017**, *7*, 49–55. [Pdf], [Publisher]

[14] G.A. Khalid, Synthesis and spectrophotometric study of cobalt, nickel and copper ions complexes with some new azo dyes containing 4,5– diphenyl imidazole, *Natl. J. Chem*., **2007**, *28*, 585–602. [Google Scholar], [Publisher]

[15] R.J.H. Clark, D. Brown, The chemistry of vanadium, niobium and tantalum: Pergamon texts in inorganic chemistry, *Elsevier*, **2013**. [Crossref], [Google Scholar], [Publisher]

[16] E.R. Agharia, Infrared Spectroscopic Investigations of Effect of Strong Resonance Stabilized Intramolecular Hydrogen Bonding in 1- (1-Hydroxy-2-naphthyl)-3-(phenyl or Substituted phenyl)-prop-2-en-1-ones and on their Complexation with Some Transition Metals, *Chem. Sci*., **2015**, *4*, 463–477. [Crossref], [Google Scholar], [Publisher]

[17] M.A. Farrukh, K.M. Butt, K.-K. Chong, W.S. Chang, Photoluminescence emission behavior on the reduced band gap of Fe doping in CeO_2-SiO_2 nanocomposite and photophysical properties, *J. Saudi Chem. Soc*., **2019**, *23,* 561–575. [Crossref], [Google Scholar], [Publisher]

[18] K.Y. Qader, R.A. Ghazi, A.M. Jabbar, K.H. Abass, S.S. Chiad, Reduce of energy gap of cuo nano structure film by Ag doping, *J. Green Eng*., **2020**, *10*, 7387–7398. [Google Scholar], [Publisher]

[19] G.M. Poralan, J.E. Gambe, E.M. Alcantara, R.M. Vequizo, X-ray diffraction and infrared spectroscopy analyses on the crystallinity of engineered biological hydroxyapatite for medical application, *IOP Conf. Ser. Mater. Sci. Eng*., IOP Publishing, **2015**, 12028. [Crossref], [Google Scholar], [Publisher]

[20] S. Guggenheim, D.C. Bain, F. Bergaya, M.F. Brigatti, V.A. Drits, D.D. Eberl, M.L.L. Formoso, E. Galán, R.J. Merriman, D.R. Peacor, Report of the Association Internationale pour l'Etude des Argiles (AIPEA) Nomenclature Committee for 2001: Order, disorder and crystallinity in phyllosilicates and the use of the 'Crystallinity Index', *Clay Miner*., **2002**, *37*, 389–393. [Crossref], [Google Scholar], [Publisher]

[21] S.K. Mishra, H. Roy, A.K. Lohar, S.K. Samanta, S. Tiwari, K. Dutta, A comparative assessment of crystallite size and lattice strain in differently cast A356 aluminium alloy, *IOP Conf. Ser. Mater. Sci. Eng*., IOP Publishing, **2015**, 12001. [Crossref], [Google Scholar], [Publisher]

[22] M. Rabiei, A. Palevicius, A. Monshi, S. Nasiri, A. Vilkauskas, G. Janusas, Comparing methods for calculating nano crystal size of natural hydroxyapatite using X-ray diffraction, *Nanomaterials*., **2020**, *10*, 1–21. [Crossref], [Google Scholar], [Publisher]

[23] N.K. Chaudhary, B. Guragain, S.K. Chaudhary, P. Mishra, Schiff base metal complex as a potential therapeutic drug in medical science: A critical review, *Bibechana*., **2021**, *18*, 214–230. [Google Scholar], [Publisher]

[24] J. Courtois, B. Wang, W.S. Abdul-Hassan, L. Almásy, M. Yan, G. Royal, Redox-responsive colloidal particles based on coordination polymers incorporating viologen units, *Inorg. Chem*., **2020**, *59*, 6100–6109. [Crossref], [Google Scholar], [Publisher]

[25] A.B.P. Lever, S.I. Gorelsky, Ruthenium complexes of non-innocent ligands: Aspects of charge transfer spectroscopy, *Opt. Spectra Chem. Bond. Transit. Met. Complexes*., **2004**, 77–114. [Crossref], [Google Scholar], [Publisher]

[26] J. Abdelhak, S. Namouchi Cherni, M. Amami, H. El Kébir, M.F. Zid, A. Driss, Iron (III) and cobalt (III) complexes with oxalate and phenanthroline: synthesis, crystal structure, spectroscopy properties and

magnetic properties, *J. Supercond. Nov. Magn*., **2014**, *27*, 1693–1700. [Crossref], [Google Scholar], [Publisher]

[27] D. Sado, Y. Gaëlle, D.M. Yufanyi, R. Jagan, M.O. Agwara, Synthesis, characterization and antimicrobial properties of cobalt(II) and cobalt(III) complexes derived from 1,10-phenanthroline with nitrate and azide co-ligands, *Cogent Chem*., **2016**, *27*, 1253201. [Crossref], [Google Scholar], [Publisher]

[28] W.S. Abdul-Hassan, D. Roux, C. Bucher, S. Cobo, F. Molton, E. Saint-Aman, G. Royal, Redox-triggered folding of self-assembled coordination polymers incorporating Viologen Units, *Chem. - A Eur. J*., **2018**, *24*, 12961–12969. [Crossref], [Google Scholar], [Publisher]

[29] J. Courtois, B. Wang, W.S. Abdul-Hassan, L. Almásy, M. Yan, G. Royal, Redox-responsive colloidal particles based on coordination polymers incorporating Viologen Units, *Inorg. Chem*., **2020**, *59*, 6100–6109. [Crossref], [Google Scholar], [Publisher]

How to cite this article: Haider Hussain Alia*, Wathiq Sattar Abdul-Hassan. Viologen molecular switches incorporating bis(acetylacetonato) cobalt(II) and bis(3-chloroacetylacetonato) cobalt (II) complexes. *Journal of Medicinal and Pharmaceutical Chemistry Research*, 2023, 5(7), 616-641.